Inductive Cascaded Quadruplet With Diagonal Cross-Coupling in Rectangular Waveguide

SANTIAGO COGOLLOS[1], **(Member, IEEE), RICHARD J. CAMERON**[2], **(Life Fellow, IEEE),**
MARCO GUGLIELMI[3], **(Life Fellow, IEEE), JUAN CARLOS MELGAREJO**[4],
AND VICENTE E. BORIA[1], **(Fellow, IEEE)**

[1]Departamento de Comunicaciones, Universitat Politècnica de València, 46022 Valencia, Spain
[2]ComDev Europe, Aylesbury HP22 5SX, U.K. *(Retired)*
[3]Instituto de Telecomunicaciones y Aplicaciones Multimedia, iTEAM, Universitat Politècnica de València, 46022 Valencia, Spain
[4]Cambrian Intelligence, London EC1M 7AD, U.K.

Corresponding author: Santiago Cogollos (sancobo@dcom.upv.es)

ABSTRACT The objective of this paper is to show how inductive quadruplets with diagonal cross-couplings can be used as building blocks for filters in rectangular waveguide. Starting with the coupling matrix synthesis, we show how very general transfer functions can be easily implemented with a very simple step-by-step procedure. In addition to coupling matrix theory, we also describe distributed networks that can be effectively used to carry out the transition from coupling matrix descriptions to actual waveguide structures. Several filter design examples are also described in detail. Finally, measured results are also discussed showing excellent agreement with simulations, thereby fully validating both the new family of filter structures and the related design procedures.

INDEX TERMS Circuit synthesis, coupling matrix, diagonal cross-coupling, distributed parameter circuits, doublets, filters, inductive waveguide filters, quadruplets, space mapping.

I. INTRODUCTION

From the very early days of microwaves, the design and development of waveguide filters has always motivated a great deal of research [1]. This is because waveguide filters have always been, and still are, one of the key components of all communication systems for both ground and space applications [2]. Satellite communication systems, in particular, have always required complex filtering and multiplexing networks. Recently, however, the architecture of communication satellites is evolving from the traditional bent-pipe configuration to complex multi-beam systems, where the hardware complexity is moved to the satellite front end [3]. As a consequence, more advanced filter structures need to be developed that are suitable for integration with other front end components [4], [5].

The basic configuration used throughout this article is a quadruplet with one diagonal cross-coupling (see Fig. 1 left). The routing diagram of the modified quadruplet (MQ) is indeed similar to one of the modified doublet (MD)

The associate editor coordinating the review of this manuscript and approving it for publication was Qi Luo.

(see Fig. 1 right). The main difference between the two is that non-resonating nodes (NRNs) in the doublet are substituted by resonant nodes (RNs) in the quadruplet.

The objective of this paper is to discuss in detail the design of a new family of inductive waveguide filters in rectangular waveguide based on cascaded MQs. The key building block of the structures that we describe is a single-mode inductive quadruplet in rectangular waveguide that includes also a diagonal cross-coupling. However, before discussing the filter structures that we propose, we find it appropriate to first review the state-of-the-art of classical doublet configurations.

A review of past contributions discussing basic doublets indicates that early configurations, such as the one described in [6], did not include the cross-coupling connecting nodes 1 and 4 in Fig. 1 (right side). As a result, NRNs 1 and 4 were not directly connected. With this configuration, the basic doublet can only produce one transmission zero (TZ). The main feature of the topology discussed in [6] is the TZ switching property. Namely, that a TZ can be moved from one side to the other of the passband. This result was achieved by modifying only the resonator frequencies, without changing the couplings. However, one of the four couplings of the doublet
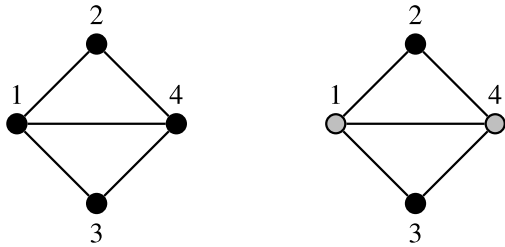
FIGURE 1. Basic modified quadruplet (left), where all nodes are RNs. Basic modified doublet (right), where nodes 1 and 4 are NRNs.

needed to have opposite sign with respect to the others. The concept was extended to other coupling topologies in [7].

The first time that the modified doublet (MD) has been discussed in the literature is in [8]. In that contribution, it was shown that it is indeed possible to generate two TZs. However, in [8] only the synthesis part of the isolated MD was discussed, and mixed signs in the coupling scheme were still required.

It is important to remark at this point that practical waveguide implementations of doublets based on dual-mode configurations without source-load couplings, were already reported in previous works, namely, [9] and [10], but without using an explicit term for the topologies. Furthermore, an additional contribution based on a rectangular waveguide dual-mode resonator as a basic doublet, where all couplings are implemented with inductive posts, can be found in [11].

Further works on advanced coupling topologies for doublets, and their practical realizations, can also be found in the literature. For instance, the extended doublet, based on connecting an additional resonant node to the node 2 of the basic MD in Fig. 1, (right), as well as the cascaded or conjoined connections of this new basic building block, were successfully discussed in [12]. Waveguide implementations using TM dual-mode cavities, where the two resonant modes of each cavity are properly excited with rotated irises, were proposed in [13]. Rectangular waveguide cavities loaded with central posts, where two closely resonant modes are used in each cavity, were also recently described in [14].

The possible implementation of doublets in substrate integrated waveguide (SIW) technology has also been widely investigated. In [15], for instance, the SIW implementation of a basic doublet structure, based on the waveguide solution discussed in [10], is described. An important additional contribution given in [15] is that the authors demonstrate how it is also possible to obtain a dual-band filter response by inserting a TZ in the center of the pass band.

The practical realization of MDs in SIW technology has also been successsfully proved in [16], where a transversal filter with high selectivity is proposed. Finally, an alterantive SIW structure that is partially filled with air, has also been proposed to implement a MD [17].

More recently, novel 3D structures based on additive manufacturing techniques have also been investigated [18]–[20],

where the basic building block is a doublet or a modification thereof.

All the filters mentioned up to this point require specific coupling techniques to implement the desired doublet structures, including, sometimes, the presence of two resonances in one cavity (in the case of dual-mode cavities) that need to be controlled simultaneously. Moreover, the final design and tuning of the resulting filters can become rather difficult, due to the simultaneous effects of one physical dimension on several coupling values. Additionally, when using MDs, it is normally observed that the coupling levels required between RNs and the source (and load) are typically very strong [13], due to the presence of NRNs. This coupling requirement, that becomes even more demanding for filters with wider bandwidth, can be alleviated with the use of a MQ where all nodes are resonant.

It would therefore be very convenient if simpler structures could be found to easily implement the MQ topology. A solution that addresses this problem in planar microstrip technology has indeed been recently proposed in [21]. However, to the authors' knowledge, no contribution can be found in the technical literature where a simple, all inductive structure in rectangular waveguide technology is proposed for implementing quadruplets with a diagonal cross-coupling. The presence of the cross coupling is a small but very significant detail, because it is indeed this cross coupling that allows the quadruplet structure to become the basis for the implementation of a very large variety of transfer functions.

The main advantages of realizing MQs, like the one shown in Fig. 1 left, with all inductive rectangular waveguide structures, with respect to the other implementations discussed are:

1) A MQ can produce two more poles per quadruplet than a doublet. This increases the overall selectivity of the filter response.
2) The inductive waveguide implementation, based on single-mode resonators, produces simple structures that are easy to design, fast to simulate with high precision, and easy to manufacture with standard milling techniques.
3) Couplings and resonant frequencies are controlled by individual geometrical features. As a consequence, the filters can be rapidly optimized, and the sensitivity of the manufactured filter to mechanization errors is significantly lower.
4) Flexible transfer functions are easily achieved with TZs at either side of the passband, based on basic sections that can then be cascaded or conjoined.
5) Reasonable coupling values and physical dimensions are obtained for the layout, even for demanding specifications.
6) The mixed signs in the topology can be implemented always with an overall all-inductive structure. Moreover, negative signs in the coupling matrix (CM) can be reduced to a minimum.

In this context, therefore, the objective of this paper is to further extend the state-of-the-art of advanced filtering structures based on the quadruplet topology in rectangular waveguide by discussing:

1) A systematic, step-by-step procedure to go from a set of specifications to a CM description for MQ configurations.
2) The detailed procedure to go from the CM representation to equivalent circuits based on distributed elements. This step will allow the definition of the starting the physical dimensions with a systematic procedure using a low number of variables in the optimization stage.
3) A number of design examples to illustrate in detail the variety of complex filtering transfer functions that can be implemented with the structures that we propose.
4) The comparisons between simulations and measured results for two filter breadboards realized following our design procedure.

The value of the results presented in this paper is, in our opinion, in the fact that the filters discussed are implemented using simple inductive structures in rectangular waveguide. As a result, they are very simple to simulate, manufacture, and integrate with other waveguide components. Furthermore, they allow for the implementation of virtually any advanced filter transfer function, thereby becoming ideal candidates for the implementation of modern payloads for both ground and space applications.

This article is organized as follows: Section II provides the guidelines to obtain the coupling matrix and routing diagrams from the specifications. Section III shows how to derive the distributed models for the filters. Section IV deals with the design of two prototypes, and the measured results are shown in section V. Section VI outlines the conclusions of this work. In appendix A the required formulas for the impedance scaling are derived. Finally, appendix B has been added to provide a comprehensive list of acronyms used throughout this article.

II. COUPLING MATRIX MODELS

The starting point for the synthesis of the CM is the set of desired filter performance specifications. The next step is normally the definition of a polynomial representation of the filter transfer function that satisfies the given specifications. Once the polynomials are defined, a canonical form must be chosen to operate the transformations producing the final topology. These transformations make use of pivots and angle rotations (in terms of the elements M_{ij} of the CM) in the classical form as described in detail in [2], for instance. The work described in this paper relies on the arrow form that is also described in [2]. From the arrow form, suitable transformations are applied to produce a topology of conjoined triplets shown in Fig. 2, where four conjoined triplets are shown as an example. A more detailed description of all the required computations can be found in [2] and [22].
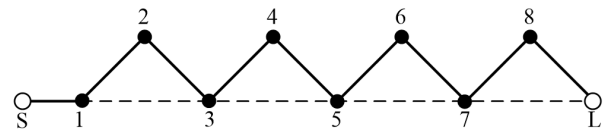

FIGURE 2. Coupling/routing schematic after the creation of 4 conjoined triplets from an arrow form.
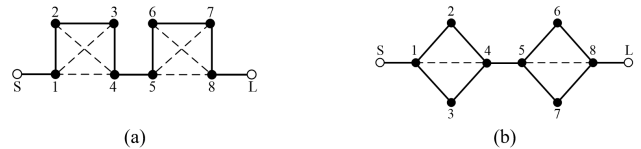

FIGURE 3. Cascaded modified quadruplet formation. (a) Cascaded quadruplets with two diagonal cross-couplings. (b) Annihilation of M_{23} and M_{67} to form two cascaded modified quadruplets.

Further rotations may now be applied to merge pairs of adjacent triplets to form quadruplets [23]. For example the first two triplets 123 and 345 may be merged into the quadruplet 1234 by a rotation at pivot [3, 4] and angle $\theta = \arctan(M_{35}^{(5)}/M_{45}^{(5)})$, so annihilating $M_{35}^{(5)}$. Similarly triplets 567 and 78L may be merged into the quadruplet 5678 by a rotation at pivot [7, 8] and angle $\theta = \arctan(M_{7L}^{(5)}/M_{8L}^{(5)})$, so annihilating $M_{7L}^{(5)}$ (see Fig. 3(a)).

Now each quadruplet with two diagonal cross-couplings may be transformed into a modified quadruplet by one further rotation. For the first quartet this means annihilating M_{23} with a cross-pivot rotation at [2, 3] and angle $\theta = 0.5 \arctan[2M_{23}/(M_{33} - M_{22})]$, similarly for the second quadruplet with a pivot at [6, 7], and so on (see Fig. 3(b)).

Conjoined modified quadruplets may be formed by pulling the second pair of triplets up the diagonal by one extra position before forming the quadruplet with two diagonal cross-couplings (Fig. 4(a)). Now the quadruplets share a common node (node 4), before the modified quadruplets are formed by annihilating M_{23} and M_{56} with cross pivot rotations [2, 3] and [5, 6] respectively (Fig. 4(b)). Note that the conjoined form only needs a 7th degree characteristic to realize 4 TZs.

A. ILLUSTRATIVE EXAMPLE

An example is given of the design of a modified quadruplet pair realizing an asymmetric seventh degree characteristic, with 23 dB return loss and with four TZs
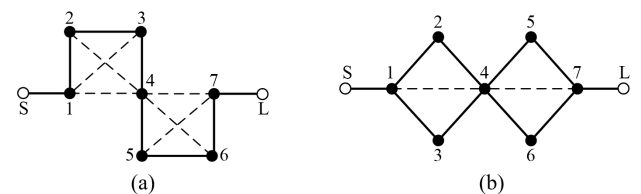

FIGURE 4. Conjoined modified quadruplet formation. (a) Conjoined quadruplets with two diagonal cross-couplings. (b) Annihilation of M_{23} and M_{56} to form two conjoined modified quadruplets.
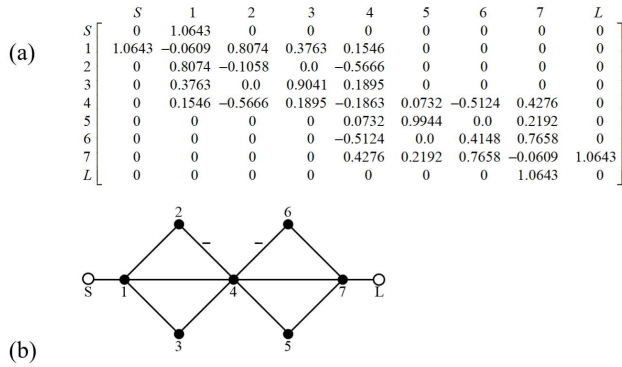
(a)

	S	1	2	3	4	5	6	7	L
S	0	1.0643	0	0	0	0	0	0	0
1	1.0643	−0.0609	0.8074	0.3763	0.1546	0	0	0	0
2	0	0.8074	−0.1058	0.0	−0.5666	0	0	0	0
3	0	0.3763	0.0	0.9041	0.1895	0	0	0	0
4	0	0.1546	−0.5666	0.1895	−0.1863	0.0732	−0.5124	0.4276	0
5	0	0	0	0	0.0732	0.9944	0.0	0.2192	0
6	0	0	0	0	−0.5124	0.0	0.4148	0.7658	0
7	0	0	0	0	0.4276	0.2192	0.7658	−0.0609	1.0643
L	0	0	0	0	0	0	0	1.0643	0

(b)

FIGURE 5. 7-4 asymmetric modified quadruplet pair. (a) Coupling matrix. (b) Coupling/routing diagram.

	S	1	2	3	4	5	6	L	
S	M_{SS}	M_{S1}	M_{S2}	M_{S3}	M_{S4}	M_{S5}	M_{S6}	M_{SL}	
1	·	M_{11}	M_{12}	M_{13}	M_{14}	M_{15}	M_{16}	M_{1L}	
2	·	·	M_{22}	M_{23}	M_{24}	M_{25}	M_{26}	M_{2L}	
3	·	·	·	M_{33}	M_{34}	M_{35}	M_{36}	M_{3L}	Cross- Couplings
4	·	·	·	·	M_{44}	M_{45}	M_{46}	M_{4L}	
5	·	·	·	·	·	M_{55}	M_{56}	M_{5L}	
6	·	·	·	·	·	·	M_{66}	M_{6L}	Main-Line Couplings
L	·	·	·	·	·	·	·	M_{LL}	Self Couplings

FIGURE 7. Sign changes for filtering characteristic reversal. Any coupling on the dashed diagonal lines will change sign but not value.

at $-j1.9442$, $-j1.3517$, $-j1.1731$ and $-j1.1162$ to give four 60 dB rejection lobes on the lower side of the passband. After synthesizing the arrow coupling matrix, four triplets are formed on the diagonal of the coupling matrix, merged in pairs and then the couplings M_{23} and M_{56} annihilated. The resultant coupling matrix and corresponding coupling and routing diagram are shown in Fig. 5, and the rejection and RL performance are shown in Fig. 6.
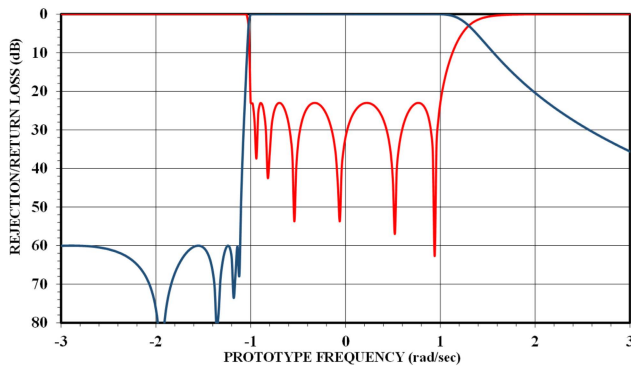

FIGURE 6. 7-4 asymmetric modified quadruplet pair. Rejection and return loss performance.

In the coupling matrix of Fig. 5, positive or negative mainline and cross-couplings are realized with appropriately dimensioned and positioned aperture and resonator widths as will be explained in Section IV-A. The signs and values of the self-couplings on the diagonal of the CM are realized with offsets from the filter center frequency of the resonant frequencies of the cavities: a negative value for the self-coupling means a resonant frequency offset above the filter center frequency for the corresponding resonator, and vice versa.

B. REVERSAL OF THE FILTERING CHARACTERISTIC
The reversal (mirroring about center frequency) of a filter's characteristic is sometimes used for the design of contiguous-channel diplexers, being useful in that the first filter design may be used for the s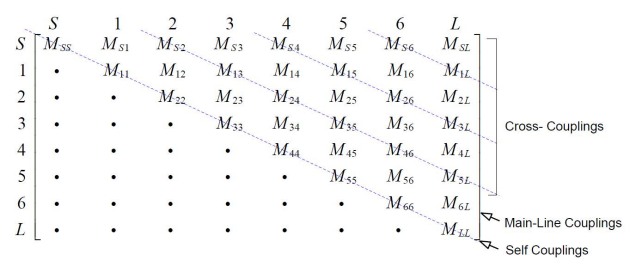econd diplexer filter, requiring only a retuning of the resonators and the change of sign of some of the couplings of the second filter. Otherwise their absolute values are the same.

For any bandpass or bandstop prototype, it is possible to reverse its filtering characteristics simply by retaining the original absolute value but changing the sign of any self- or inter-resonator coupling value in the matrix whose indices add to an even integer. For example coupling M_{22} (a self-coupling) or M_{24} (a cross-coupling) would change sign, but M_{12} (a main-line coupling) or M_{14} would not. For this purpose, index 'S' is replaced with zero and index 'L' with '$N + 1$'. This procedure may be visualized by drawing the principal diagonal on the coupling matrix, and then alternate parallel diagonals until the upper-right and lower-left corners of the matrix are reached (see Fig. 7).

This means that the self-couplings always change sign (conjugate) whilst main-line couplings retain their original sign. For a triplet one cross coupling will change sign, whilst two will change in a modified quadruplet. These coupling sign changes may be moved to other couplings in the matrix or reduced in number by the method of enclosures [2].

III. DISTRIBUTED MODELS
The MQ cell can be directly translated into a distributed model (DM), or network, using admittance inverters and lengths of transmission lines. This distributed network then becomes a very effective tool to perform the transition from a CM description to an actual waveguide device. The transition can, in fact, be accomplished by using the DM to obtain a number of reference curves for portions of the network. The various reference curves can then be used to obtain the initial dimensions of a real waveguide structure. The DM that we propose to use to represent the MQ is shown in Fig. 8.

It is important to note that, in Fig. 8, all inverters and transmission lines have the same common ground that is, therefore, omitted in the drawing. The connection to ground in the transmission lines means that they are terminated with a short circuit. Furthermore, all internal lines have the same characteristic impedance. Finally, the input and output lines can also have the same characteristic impedance if J_{S1} and J_{4L} are suitably scaled. In fact, the whole circuit can be impedance scaled to have all lines with $Z_0 = 1\,\Omega$, if required.
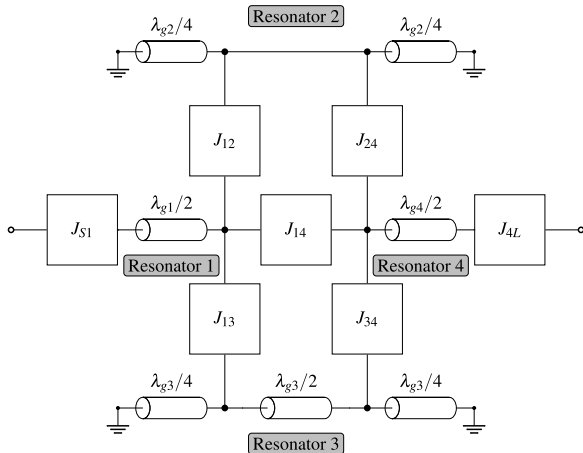
FIGURE 8. Distributed model for a modified quadruplet (4 RNs with 1-4 coupling).

As we can see in Fig. 8, the total length of resonator 3 is one wavelength, whereas the other three resonators are half wavelength long. This is done, as will be explained in more detail later on, to implement the negative coupling required in the basic MQ cell.

Next, we show how the DM can be easily transformed into a lumped element network, and how the values of the DM elements are related to the entries of the CM of the MQ cell.

A. THE EQUIVALENT NETWORK OF A TRANSMISSION LINE

It is well known that distributed transmission lines with lengths $\lambda/4$ and $\lambda/2$ can be represented by the lumped element networks shown in Fig. 9, where

$$L_p = \frac{4Z_0}{\pi\omega_0}; \quad C_p = \frac{\pi Y_0}{4\omega_0}; \quad L_s = \frac{\pi Z_0}{2\omega_0}; \quad C_s = \frac{2Y_0}{\pi\omega_0} \quad (1)$$

The formulas in (1) are derived following the same approach explained in detail in [24]. The transformer accounts for the phase reversal of the signal in a half-wavelength transmission line. This phase behavior is crucial since it allows to implement the negative couplings required in the MQ using only positive admittance inverters in the DM.

It is important to note that resonators 1 and 4 in Fig. 8 are half-wavelength long. The phase reversal that they introduce could be included in J_{S1} and J_{4L} but, since the sign on these inverters can be changed arbitrarily without changing the response (method of enclosures [2]), we can ignore this phase reversal. Furthermore, the short circuits at the end of the quarter-wavelength transmission lines cancel one of the parallel resonators, as well as the inverters of the lumped element networks in Fig. 9. Another approximation that we have used is to neglect the series resonators $L_s - C_s$, since we assume that the inverter values are small for practical filters.

Finally, therefore, the resulting (approximate) lumped element network that we obtain from the DM is shown
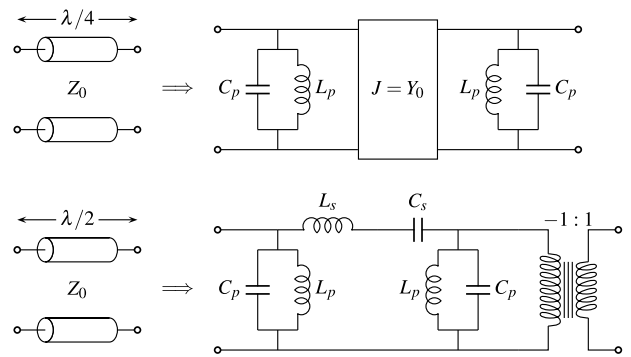

FIGURE 9. Equivalent circuits for quarter-wavelength and half-wavelength transmission lines near resonance.
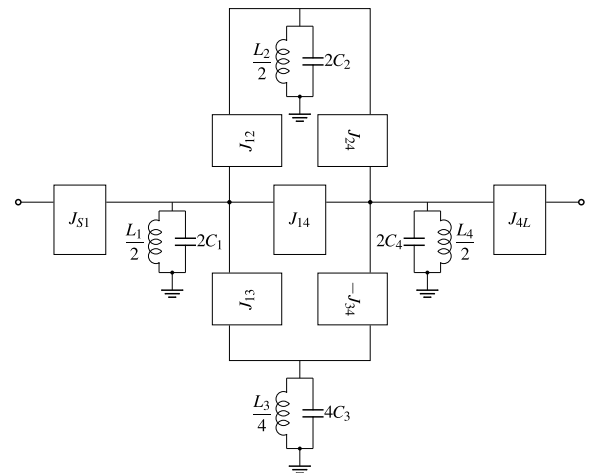

FIGURE 10. Lumped element equivalent network obtained from the DM.

in Fig. 10, where the phase reversal due to resonator 3 has been embedded in the inverter J_{34}. The reason for having resonator 3 longer than resonator 2 is to implement the negative coupling that is required by the modified quadruplet topology. As a consequence, all inverters in the DM can be positive, while the couplings in the lumped element model have different signs. For the sake of clarity, the total length of any resonator in the DM gives the mode used for the corresponding resonance: resonators with length $\lambda_g/2$ use the TE_{101}, resonators with length λ_g use the TE_{102} and so on.

The capacitance and inductance values of the resonators in Fig. 10 are different for each resonator since, in general, every resonator resonates at its own ω_{0i}. We can therefore write:

$$\omega_{0i} = \frac{1}{\sqrt{L_i C_i}}, \quad i = 1, 2, 3, 4 \quad (2)$$

where

$$L_i = \frac{4}{\pi\omega_{0i}}, \quad C_i = \frac{\pi}{4\omega_{0i}}, \quad i = 1, 2, 3, 4 \quad (3)$$

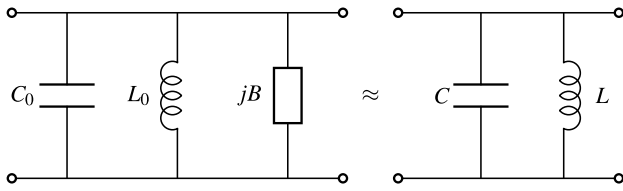Note that, for the sake of clarity, we have assumed that $Z_0 = 1\,\Omega$ without loss of generality.

FIGURE 11. Equivalent circuit representing the resonators in the coupling matrix (left). Equivalent resonator without FIRs (right).
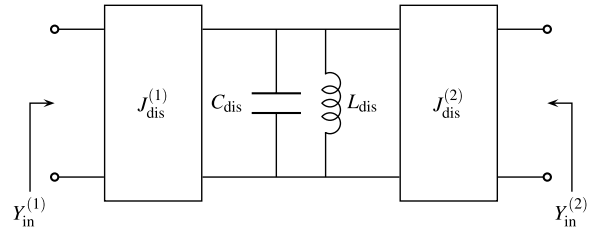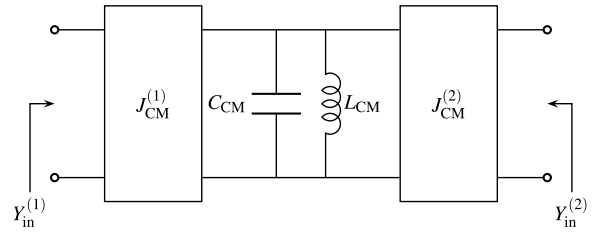

FIGURE 12. Resonator obtained from the CM with adjacent inverters (top). Resonator obtained from the simplification of the distributed model with adjacent inverter (bottom).

B. SCALING THE MODEL

Once all resonators are replaced by lumped elements, we are ready to identify the elements of the circuit in Fig. 10 with the elements of the CM. To do that, we first assume that the CM produces an equivalent circuit with resonators in the form of parallel lumped elements with normalized values for the capacitors in the low-pass model. The transition from low-pass to bandpass is then given by the usual lowpass-to-bandpass transformation, resulting in the equivalent circuit shown in the left of Fig. 11. We now note that B is the value of the frequency independent reactance (FIR), that comes from the diagonal elements of the CM corresponding to the resonators, and is not affected by the frequency transformation.

The next step is to eliminate the FIRs (see Fig. 11 right). The procedure is straightforward. Since we have two elements L and C we need the two usual conditions: the same resonant frequency ω_0 and the same slope parameter $\mathcal{B}$. The slope parameter of the circuit in the left side of Fig. 11 is given by

$$
\begin{aligned}
\mathcal{B} &= \frac{\omega_0}{2} \frac{d\Im\{Y_{\text{in}}\}}{d\omega}\bigg|_{\omega=\omega_0} \\
&= \frac{\omega_0 C_0}{2} + \frac{1}{2\omega_0 L_0} \\
&= \frac{1}{\omega_0 L_0} - \frac{B}{2} \\
&= \frac{B}{2} + \omega_0 C_0
\end{aligned}
\tag{4}
$$

where ω_0 cancels the imaginary part of the admittance of the resonator, that is $B + \omega_0 C_0 - 1/(\omega_0 L_0) = 0$, while for the circuit on the right side of Fig. 11 we have simply $\mathcal{B} = \omega_0 C$ and $\omega_0 = 1/\sqrt{LC}$. Equating both expressions for the slope parameter, we have

$$
\begin{aligned}
C &= \frac{1}{\omega_0}\left(C_0\omega_0 + \frac{B}{2}\right) \\
L &= \frac{1}{\omega_0}\left(C_0\omega_0 + \frac{B}{2}\right)^{-1}
\end{aligned}
\tag{5}
$$

We now note that the values of C_0 and L_0 are the usual ones given by the lowpass-to-bandpass transformation applied to a capacitor of value equal to 1 F, so that

$$
C_0 = \frac{1}{\Delta\omega} \qquad L_0 = \frac{\Delta\omega}{\omega_0^2}
\tag{6}
$$

where $\Delta\omega = 2\pi BW$ and BW is the filter frequency bandwidth.

The last step is to identify the lumped element model given by the CM and the lumped element model obtained after simplifying the DM. In this context, it is enough to identify each block inverter-resonator-inverter to obtain the proper scaling. Let us use the subscript 'dis' for the block coming from the distributed model, and the subscript 'CM' for the circuit coming from the coupling matrix. We now write

$$
\begin{aligned}
C_{\text{CM}} &= \frac{1}{\omega_0}\left(\frac{\omega_0}{\Delta\omega} + \frac{B}{2}\right) \\
C_{\text{dis}} &= \frac{\pi}{2\omega_0}
\end{aligned}
\tag{7}
$$

where C_{dis} is the value of the capacitor for the half-wavelength resonators. If the resonator has length λ_g, then the expression of C_{dis} in (7) has to be multiplied by two as shown in Fig. 10. The expressions of L_{CM} and L_{dis} are obtained imposing the resonance at ω_0, namely $L = 1/(C\omega_0^2)$.

To obtain the admittance looking into port $i = 1, 2$ (see Fig. 12), we assume a short circuit termination at the other access, as it is customary to obtain an admittance matrix. Enforcing the same admittance values, we obtain

$$
\begin{aligned}
Y_{\text{in}}^{(i)} &= \frac{J_{\text{CM}}^{2\,(i)}}{j\omega C_{\text{CM}} + \dfrac{1}{j\omega L_{\text{CM}}}} = \frac{J_{\text{dis}}^{2\,(i)}}{j\omega C_{\text{dis}} + \dfrac{1}{j\omega L_{\text{dis}}}} \\
&= \frac{1}{j\omega \dfrac{C_{\text{CM}}}{J_{\text{CM}}^{2\,(i)}} + \dfrac{1}{j\omega L_{\text{CM}} J_{\text{CM}}^{2\,(i)}}} \\
&= \frac{1}{j\omega \dfrac{C_{\text{dis}}}{J_{\text{dis}}^{2\,(i)}} + \dfrac{1}{j\omega L_{\text{dis}} J_{\text{dis}}^{2\,(i)}}}
\end{aligned}
\tag{8}
$$

Identifying terms we write

$$
\frac{C_{\text{CM}}}{J_{\text{CM}}^{2\,(i)}} = \frac{C_{\text{dis}}}{J_{\text{dis}}^{2\,(i)}}
\tag{9}
$$

So that we can now solve for our unknown, obtaining $J_{\text{dis}}^{(i)}$

$$J_{\text{dis}}^{(i)} = J_{\text{CM}}^{(i)} \sqrt{\frac{C_{\text{dis}}}{C_{\text{CM}}}} \qquad (10)$$

A term like (10), therefore, appears in each inverter due to one of the adjacent resonators. If one inverter has a resonator at each side, we can write the full set of equations for the relevant modified quadruplet, taking into account expressions in (7), as follows

$$J_{S1} = M_{S1}\sqrt{S_1}$$
$$J_{4L} = M_{4L}\sqrt{S_4}$$
$$J_{ij} = M_{ij}\sqrt{S_i S_j} \quad i, j = 1, 2, 3, 4 \qquad (11)$$

where

$$S_i = \frac{\pi/2}{1/\mathcal{W}_i + M_{ii}/2} \qquad (12)$$

The above equations are applicable to half-wavelength resonators. For full-wavelength resonators, however, the numerator of (12) should be replaced by π, and one of the adjacent inverters should have a sign that is the opposite of the corresponding CM element, to account for the phase reversal. Note that, for each TEM resonator $\mathcal{W}_i = \Delta\omega/\omega_{0i}$. However, for waveguide modes the guide-wavelength fractional bandwidth $\mathcal{W}_{\lambda i}$ should be used instead [1]. The formulas obtained in (11) are also valid for the cascaded and/or conjoined connections of any number (without limitation) of MQs.

In order to complete our derivation, it is also important to obtain the resonant frequency of each resonator in the CM (Fig. 11 left). This is required in order to compute the corresponding $\mathcal{W}_i$ or $\mathcal{W}_{\lambda i}$. The value of the ω_{0i}, in terms of the bandpass values L_0, C_0 and B, is given by

$$\omega_{0i} = \begin{cases} \dfrac{B}{2C_0}\left(\sqrt{1 + \dfrac{4C_0}{L_0 B^2}} - 1\right), & B > 0 \\[4mm] -\dfrac{B}{2C_0}\left(1 + \sqrt{1 + \dfrac{4C_0}{L_0 B^2}}\right), & B < 0 \end{cases} \qquad (13)$$

where both cases provide a positive value for ω_{0i}. The values for $B = M_{ii}$, L_0 and C_0 are provided by (6). One may argue that (11) and (12) have been obtained assuming that we have only one inverter at each side of a resonator. In our DM, however, there are junctions (e.g. at the output of resonator 1) where several inverters are connected in parallel. The formulas are still the same ones, as it is proven in Appendix A where the scaling at certain node is obtained with any number of inverters connected in parallel to it.

C. ILLUSTRATIVE EXAMPLE

As a simple application example for the formulas derived in the previous section, we now derive the element values for the distributed model of an asymmetric 4-2 filter with return loss $RL = 23$ dB, upper-band rejection of 30 dB, with $f_0 = 11$ GHz, and with $BW = 200$ MHz. The distributed model will be extracted for a standard waveguide WR-75 in

all resonators. The coupling matrix for this filter is (14), as shown at the bottom of the next page.

The distributed circuit is shown in Fig. 8. The resonant frequency for each resonator is given next:

$$f_{01} = f_{04} = 10.9838 \text{ GHz}$$
$$f_{02} = 11.0036 \text{ GHz}$$
$$f_{03} = 11.1033 \text{ GHz} \qquad (15)$$

and the inverter values are

$$J_{S1} = 0.2710 = J_{4L}$$
$$J_{12} = 0.0549 = J_{24}$$
$$J_{13} = 0.0256 = J_{34}$$
$$J_{14} = 0.02153 \qquad (16)$$

where all inverter values are positive, as expected. The M_{13} was originally negative but, the sign inversion is provided by resonator 3 (having a length of λ_{g3}). We could have indifferently assigned a change of sign to J_{13} or J_{34} (but not to both simultaneously). The simulation of the lumped element circuit given by the coupling matrix is compared with the distributed model response in Fig. 13. It is remarkable that such a good agreement is obtained without using any optimization. The reason is that the approximations shown in Fig. 9 are very good near resonance and, therefore, for narrowband applications these approximations are indeed of the same order as the ones used to obtain the classical formulas for in-line filters [1]. Therefore, the same limitations apply: approximations worsen when the number of resonators increases, and when the relative bandwidth increases. However, for practical orders and moderate bandwidths, (11) and (12) work with outstanding precision.
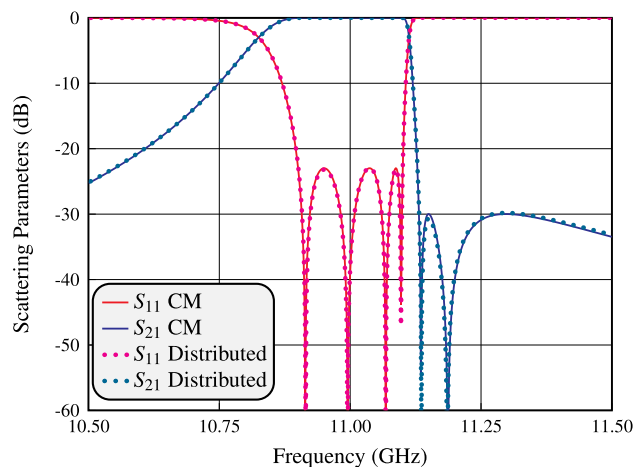

FIGURE 13. Electrical response of the lumped circuit given by the coupling matrix (solid lines) compared with the distributed circuit performance (dotted).

As reported in section II-B, it is very easy to obtain the reversal of the response given in Fig. 13. We have to change the couplings whose indices add to an even integer. Therefore, M_{13} and M_{24} will change sign in addition to all

elements of the main diagonal (17), as shown at the bottom of the page.

Additionally, as the minus sign is implemented with a λ_g resonator, the distributed model will be like the one in Fig. 8, but with the resonator 2 with length λ_{g2} and the resonator 3 with length $\lambda_{g3}/2$.

Therefore, the distributed model will have the following resonant frequency for the resonators:

$$f_{01} = f_{04} = 11.0162\,\text{GHz}$$
$$f_{02} = 10.9964\,\text{GHz}$$
$$f_{03} = 10.8977\,\text{GHz} \tag{18}$$

and the inverter values are

$$J_{S1} = 0.2706 = J_{4L}$$
$$J_{12} = 0.0775 = J_{24}$$
$$J_{13} = 0.0183 = J_{34}$$
$$J_{14} = 0.02146 \tag{19}$$

The simulation of the lumped element circuit given by the coupling matrix is compared with the distributed model response in Fig. 14, showing again a very good agreement.

IV. DESIGN EXAMPLES

The next step in the design process, after having derived a DM, is to obtain the physical dimensions of the real waveguide structure. In this work, we have chosen to implement our filters in rectangular waveguide, an the performance of all the filter structures we discuss will be obtained using full-wave electromagnetic simulators (EM model). The purpose of this section is to provide the guidelines to obtain the physical dimensions of the EM model from the DM derived in the previous section.

In this context, it is important to mention that we will use FEST3D for all the EM simulations. One particular feature of FEST3D is that the user can choose the set of computational parameters that determine the accuracy of the computations. Naturally, more accurate results require
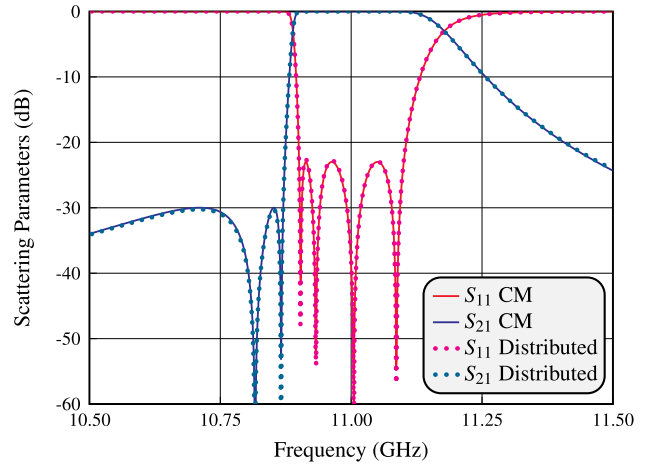

FIGURE 14. Electrical response of the lumped circuit given by the coupling matrix (solid lines) compared with the distributed circuit performance (dotted). This is the filter with the reversal response of Fig. 13.

more computation time. For the design examples discussed in this paper, FEST3D has been used in both low accuracy mode (LA) and in high accuracy mode (HA). The corresponding computational parameters are as follows:

- Accessible modes = 5 (LA), 25 (HA)
- Basis Functions = 15 (LA), 75 (HA)
- Terms in the kernel = 150 (LA), 750 (HA)

More information about the meaning of these parameters is given in [25].

A. EXAMPLE 1: 4-2 ASYMMETRIC FILTER

The simplest filter example is the basic MQ with the DM shown in Fig. 8. We will first discuss the asymmetric case with a transfer function equal to the one in Fig. 14 ($f_0 = 11$ GHz and $BW = 200$ MHz, two TZs to the left). The waveguide layout we are aiming for is the simple inductive structure (constant height) in WR-75 ($a = 19.05$ mm and $b = 9.525$ mm) shown in Fig. 15.

$$M = \begin{pmatrix} 0 & 1.11971 & 0 & 0 & 0 & 0 \\ 1.11971 & 0.16222 & 0.93803 & -0.31075 & 0.36747 & 0 \\ 0 & 0.93803 & -0.03582 & 0 & 0.93803 & 0 \\ 0 & -0.31075 & 0 & -1.02780 & 0.31075 & 0 \\ 0 & 0.36747 & 0.93803 & 0.31075 & 0.16222 & 1.11971 \\ 0 & 0 & 0 & 0 & 1.11971 & 0 \end{pmatrix} \tag{14}$$
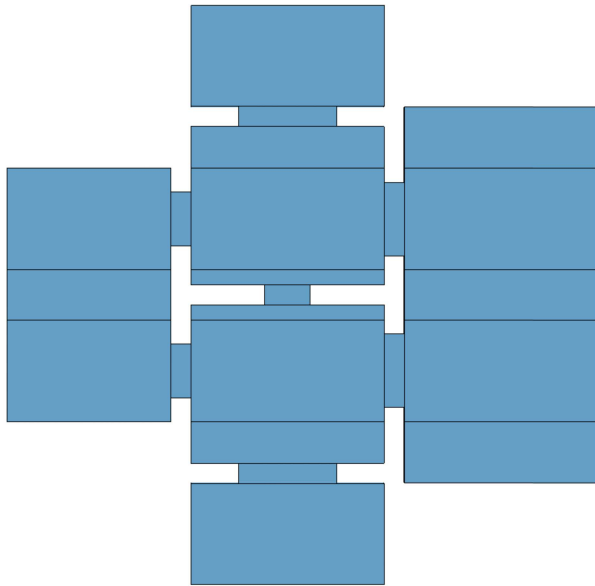
$$M = \begin{pmatrix} 0 & 1.11971 & 0 & 0 & 0 & 0 \\ 1.11971 & -0.16222 & 0.93803 & 0.31075 & 0.36747 & 0 \\ 0 & 0.93803 & 0.03582 & 0 & -0.93803 & 0 \\ 0 & -0.31075 & 0 & 1.02780 & 0.31075 & 0 \\ 0 & 0.36747 & 0.93803 & 0.31075 & -0.16222 & 1.11971 \\ 0 & 0 & 0 & 0 & 1.11971 & 0 \end{pmatrix} \tag{17}$$

FIGURE 15. Waveguide structure (top view) implementing the DM of Fig. 8.

FIGURE 16. DM1 (top) and WM1 (bottom).

FIGURE 17. Electrical responses for the structures in Fig. 16.

The first objective in our design process is to obtain a low accuracy (LA) EM model, that is computationally very efficient and that gives the exact same response as the DM.

To this end, we decompose the DM into three partial models (PMs). The PMs will be used to generate design curves representing the target performance for the corresponding LA PMs in waveguide (WMs). The procedure can be divided into the following steps:

Step 1: Design resonator 2. The DM1 model shown in Fig. 16 (top) is implemented with the WM1 structure show in Fig. 16 (bottom). The WM1 is then optimized to give the same performance of the partial DM1. The optimization requires only two variables: the window apertures (w_{12}), and the width of resonator 2 (a_2). The width has been chosen as an optimization parameter in order to have a fixed length for the central part of the structure. The responses of both circuits are compared in Fig. 17.

Step 2: Design resonator 3. The DM2 model in Fig. 18 (top) is implemented with WM2 shown in Fig. 18 (bottom). The optimization requires again only two variables: the window apertures (w_{13}) and the lengths (r_3). The responses of both circuits are compared in Fig. 19.

Step 3: Design resonator 1. The DM3 model shown in Fig. 20 (top) is implemented with the WM3 shown in Fig. 20 (bottom). The optimization requires again only three variables: the length r_1, the window apertures w_{s1} and w_{14}. The responses of both circuits are compared in Fig. 21.

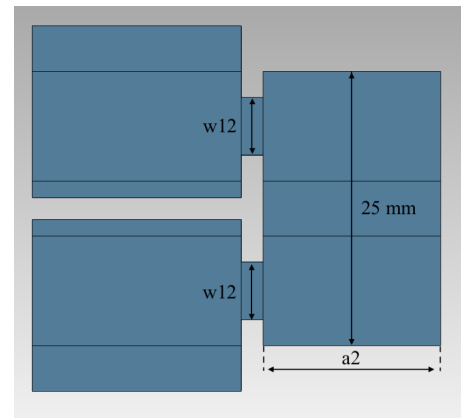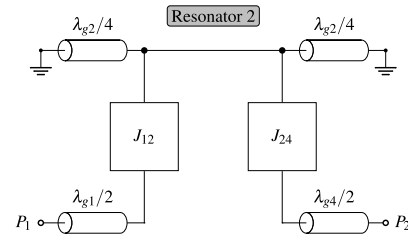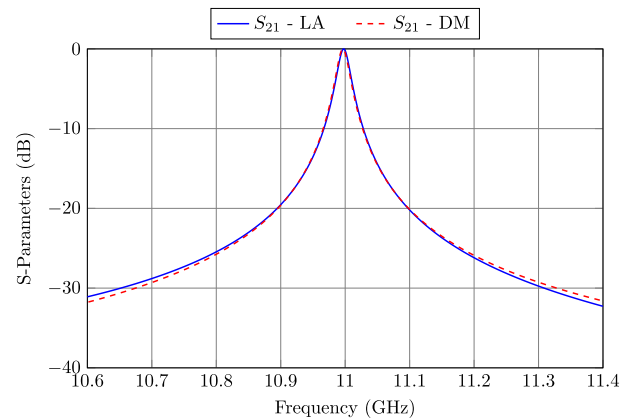We can now assemble all WMs to obtain the initial complete LA model in waveguide. Fig. 22 shows the initial response of the LA model (iter 0). Only 3 iterations of the classic Space Mapping (SM) algorithm (based on the evaluation of the Broyden matrix [26]) are now enough to obtain the response shown in Fig. 22 (iter 3).

The next step is to obtain a high accuracy (HA) model from the LA model. It is important to note that both models use the same physical structure and the same variables for the optimization. The only difference is the accuracy of the computations.

The optimization of the HA model is again carried out using the SM algorithm, but now the Broyden matrix is always equal to the identity matrix, as discussed in [27]. This procedure leads, in one single step, to the solution shown
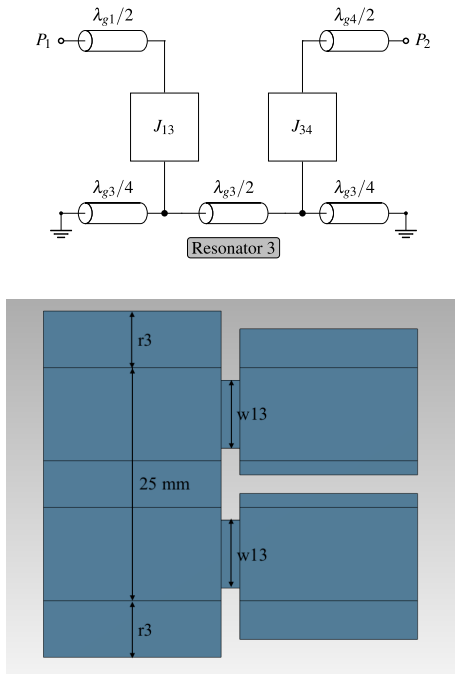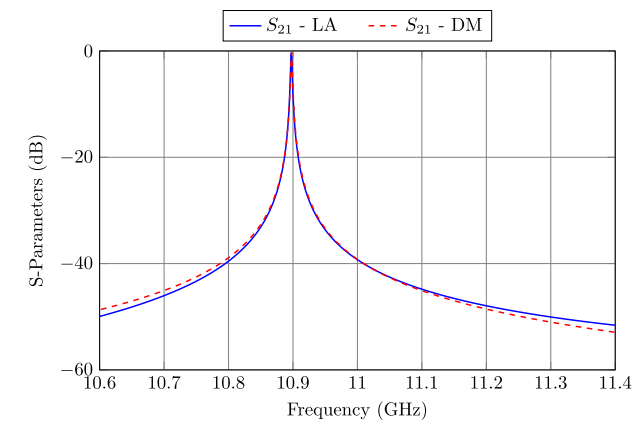
FIGURE 18. DM2 (top) and WM2 (bottom).

FIGURE 20. DM3 (top) and WM3 (bottom).

FIGURE 19. Electrical responses for the structures in Fig. 18.

FIGURE 21. Electrical responses for the structures in Fig. 20.

in Fig. 23. As we can see, we now have an excellent agreement between the HA and the DM simulations.

B. EXAMPLE 2: SYMMETRIC 7-4 FILTER

Increasing the complexity, the next structure we discuss is a symmetric 7-4 filter centered at $f_0 = 11$ GHz with bandwidth $BW = 400$ MHz, return loss $RL = 23$ dB and 60 dB rejection lobes on both sides of the passband. This example requires a pair of MQs. The routing diagram for this filter is shown in Fig. 5 (b). The responses of the coupling matrix and the DM model (see Fig. 24) are shown in Fig. 25 (top). It is interesting to note that the DM has a small deviation inside the passband, more pronounced in the lower side. This difference is due to the approximations introduced in the DM
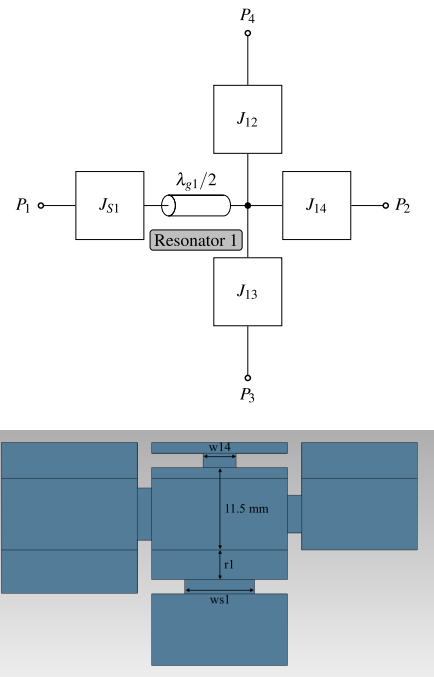
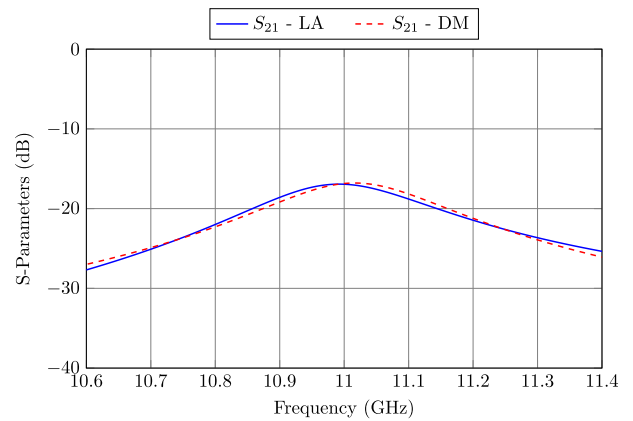derivations, and to the dispersion introduced by the WR75. We can, indeed, recover the equiripple behavior with a fast optimization, as shown in Fig. 25 (bottom), however, we now have a small shift in the location of the lower TZ.

We must also note that, for mechanical reasons, resonator number 4 is one wavelength long. This has, indeed, been taken into account in the DM, as shown in Fig. 24.

We are now ready to build the LA model for this filter, following the same procedure already described in the previous example. The first steps are exactly identical, namely, we need to match the responses of the PMs with the WMs for this filter (they are identical to the ones shown in Fig. 16, 18 and 20, respectively). However, the same process must be
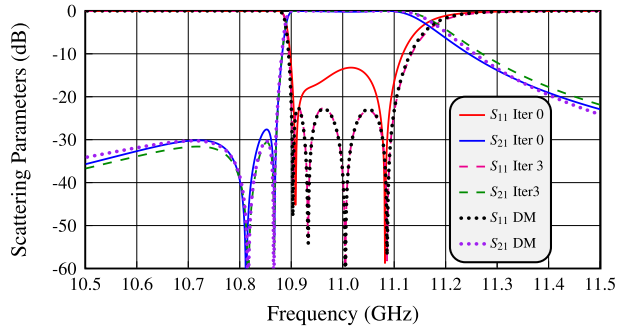
FIGURE 22. Low accuracy (LA) response for the whole filter once all parts are joined together (iter 0). After 3 iterations of SM optimization, we obtain the response in dashed line. The dotted line shows the DM response.
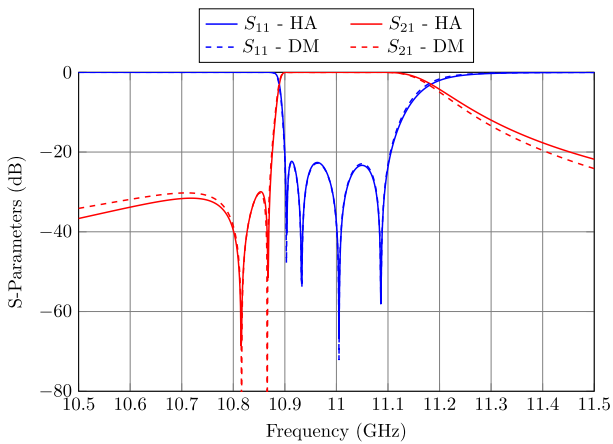

FIGURE 23. High accuracy (HA) response of the overall filter compared with the response of the DM model.
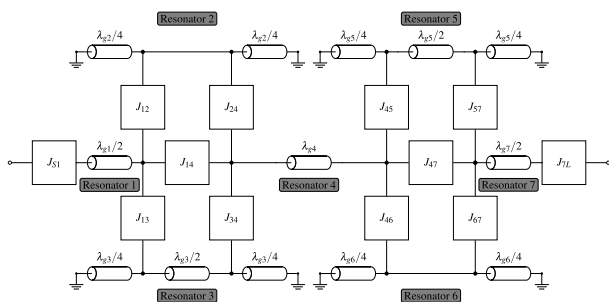

FIGURE 24. Distributed model for a 7-4 filter.

FIGURE 25. Comparison of the CM response with the DM response (top) using analytical formulas. CM vs. DM responses after recovering the equiripple in the DM through optimization (bottom).

of the complete structure. Fig 28 shows that the structure does give a good initial response (LA initial). A slight optimization is, however, needed to recover the desired response (LA final).

Finally, the HA model is obtained from the LA model following the process already discussed for the previous example. Also in this case, only one iteration is enough to obtain a compliant response. Fig. 29 shows the final HA performance compared to the DM performance.

V. EXPERIMENTAL VERIFICATION

In this section, we show the measured results obtained manufacturing the design examples discussed in the previous sections, namely, the 4-2 asymmetric filter described in subsection IV-A, and the 7-4 symmetric filter described in subsection IV-B.

Fig. 30 shows the 4-2 asymmetric filter. The filter has been manufactured using milling, and is composed of a body and a top cover. The presence of round corners, due to mechanization effects, has been considered in the HA model. It is worth mentioning that the filter does not use tuning elements, which was concluded after performing a sensitivity analysis. Fig. 31 shows the comparison between the measured response and the high accuracy simulation. As we can see, the measured response shows a very good agreement with the simulated results.

The second filter (subsection IV-B) has a more complex layout, and has also been manufactured using milling with a body and a top cover. In this case, the sensitivity analysis

used twice since we now have two MQs. The next step, once the PMs and the WMs give the same response, is to cut the DM of the complete filter in the center of resonator number 4 (see Fig. 24), and match the performances of the two new DMs obtained with the responses of the respective WMs. The results obtained with three SM iterations are shown in Fig. 26.

The next step is to assemble the two halves of the filter (the structure is shown in Fig. 27) and simulate the performance
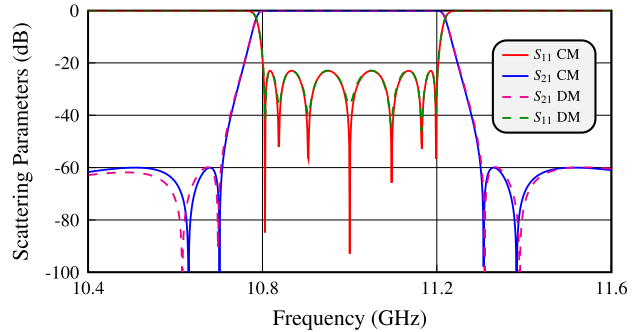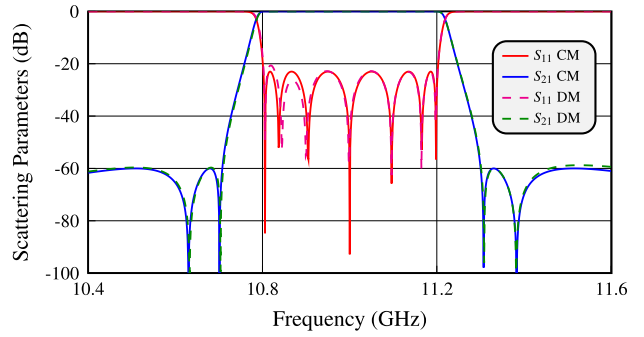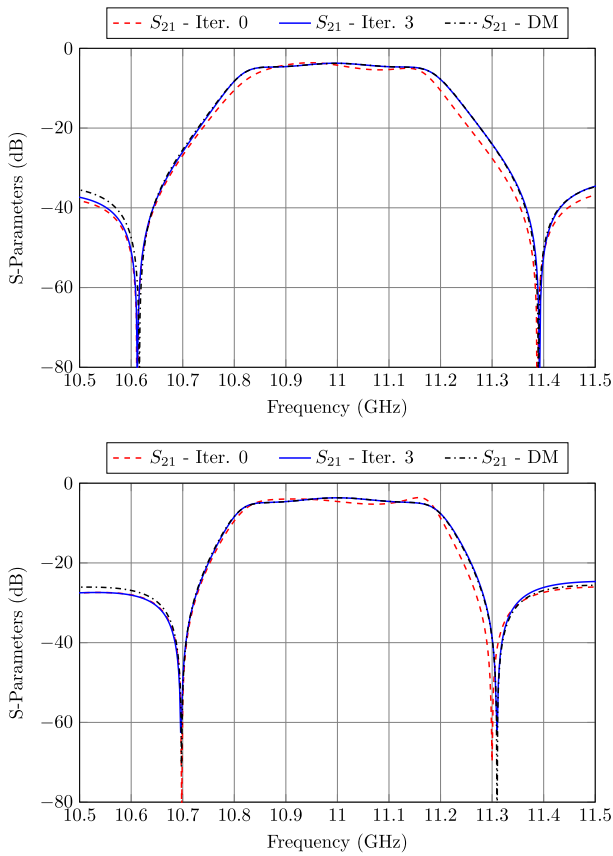
FIGURE 26. Electrical response LA (iteration 0 and iteration 3) of each half of the symmetric 7-4 filter compared with the DM.
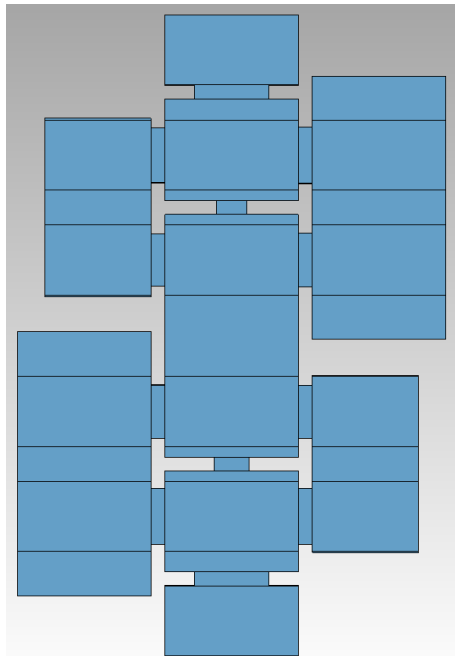

FIGURE 27. Waveguide structure (top view) implementing the DM of Fig. 24.

revealed the need of using tuning elements in all cavities and coupling windows. Screws are also used to fasten the two
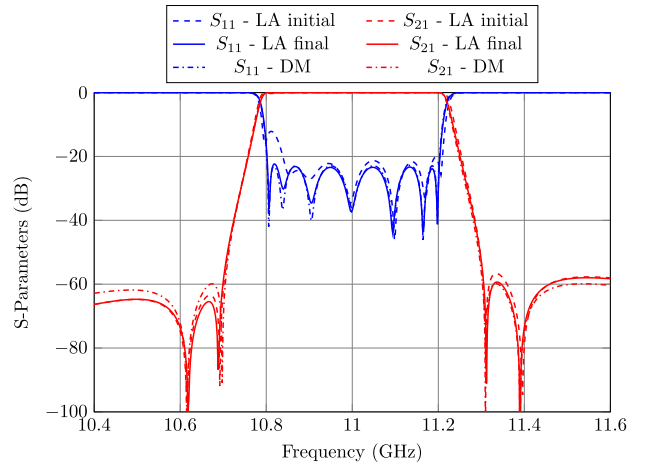

FIGURE 28. Electrical response of the complete 7-4 filter in LA compared with the DM model.

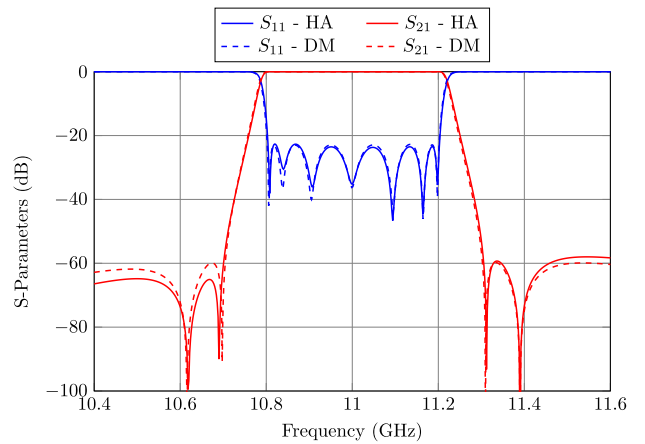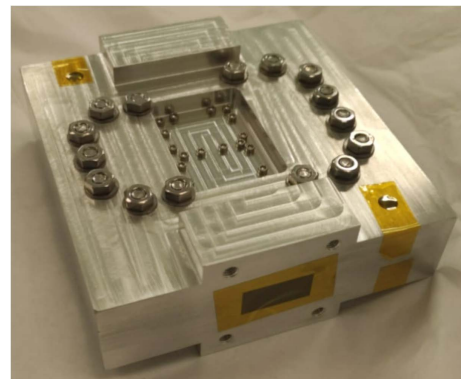**FIGURE 29.** Electrical response of the 7-4 filter in HA compared with the DM.

FIGURE 30. Manufactured 4-2 asymmetric filter.

filter's parts. The prototype (separated body and cover) is shown in Fig. 32.

Fig. 33 shows the filter performance as compared to the high accuracy simulations. The measured response is again very close to simulated data, including the very selective band edges.
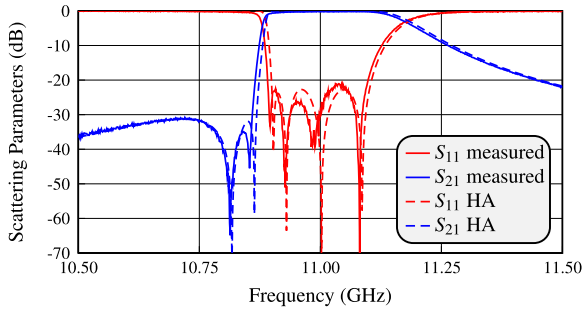
FIGURE 31. Performance of the 4-2 asymmetric filter compared with the high accuracy simulation.
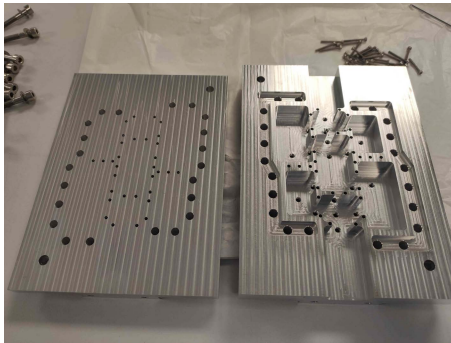

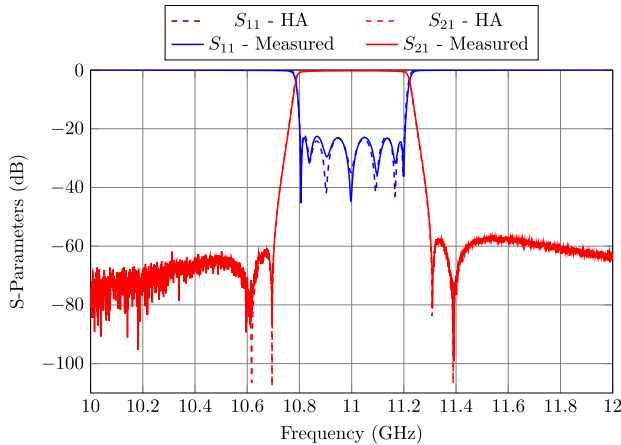**FIGURE 32.** Manufactured 7-4 symmetric filter. Top cover (left) and body (right).

FIGURE 33. Measured response of the 7-4 symmetric filter compared with the high accuracy simulation.

From the design procedure and the results obtained, we can highlight some advantages over the state-of-the-art designs: the procedure is simple even for high-order filters because cascading several MQs does not add significant complexity to the design process. The couplings are very easy to control since the structure is not overmoded, thus producing a strong independence among the different part of the filter. This also leads to a very easy segmented optimization avoiding a high number of simultaneous variables in the optimization algorithm. The prototypes are rather simple to manufacture because the structure is all-inductive.
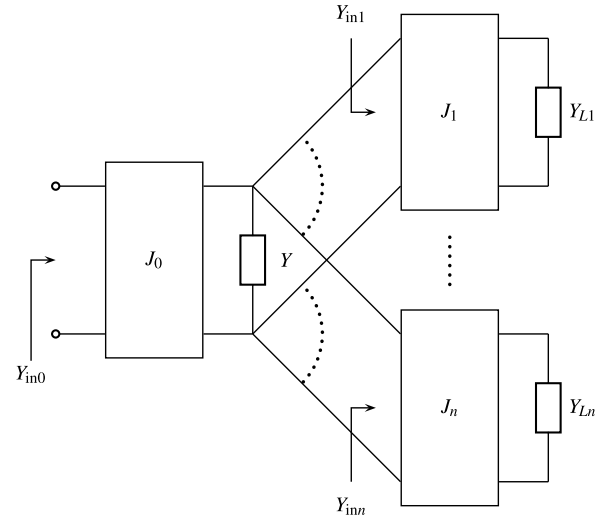

FIGURE 34. Admittance Y connected to multiple inverters.

Moreover, technical feasibility could be achieved even for very high frequencies.

VI. CONCLUSION

The objective of this paper is to describe in detail a new family of filters based on cascaded Modified Quadruplets (MQs) with diagonal inter resonator cross-couplings. Starting from the specifications, a coupling matrix is derived. Next, the coupling matrix is transformed into the canonical arrow form, and all the MQs are extracted explicitly. A lumped element circuit is then used to obtain all the parameters of a distributed model with the same performance of the original coupling matrix. The distributed model is then used to build the final full-wave EM model using a step-by-step design procedure. All the steps required to build the EM model are discussed in detail. In addition to theory, the design of two examples of increasing complexity is also discussed. Finally, two filter prototypes are designed, fabricated and measured. The measured results show an excellent agreement with the simulations, thereby fully validating the new filter family and the complete design procedure.

APPENDIX A
SCALING A NODE WITH INVERTERS IN A STAR CONFIGURATION

Let us assume that we want to normalize to unity an admittance Y that is connected to many inverters $J_0, J_1, \ldots, J_n$ in a star configuration, as shown in Fig. 34. Each inverter has a load admittance Y_{Li}.

The input admittance seen at the input of any inverter is $Y_{\text{in}i}, i = 1, \ldots, n$ and we know that

$$Y_{\text{in}i} = \frac{J_i^2}{Y_{Li}}, \quad i = 1, 2, \ldots, n \qquad (20)$$

Therefore, to compute $Y_{\text{in}0}$ we write

$$Y_{\text{in}0} = \frac{J_0^2}{Y + \sum_{i=1}^{n} Y_{\text{in}i}} = \frac{J_0^2}{Y + \sum_{i=1}^{n} \frac{J_i^2}{Y_{Li}}} \qquad (21)$$

TABLE 1. List of acronyms used in this article.

Abbr.	Meaning
CM	Coupling Matrix
DM	Distributed Model
EM	Electromagnetic
FIR	Frequency Independent Reactance
HA	High Accuracy
LA	Low Accuracy
MD	Modified Doublet
MQ	Modified Quadruplet
NRN	Non-resonating Node
PM	Partial Model
RL	Return Losses
RN	Resonating Node
SIW	Substrate Integrated Waveguide
SM	Space Mapping
TE	Transversal Electric
TEM	Transversal Electric and Magnetic
TM	Transversal Magnetic
TZ	Transmission zero
WM	Waveguide Model

which can be rewritten as

$$Y_{in0} = \frac{J_0^2/Y}{1 + \sum_{i=1}^{n} \frac{J_i^2/Y}{Y_{Li}}} = \frac{J_0'^2}{1 + \sum_{i=1}^{n} \frac{J_i'^2}{Y_{Li}}} \quad (22)$$

where the new values of the inverters when the admittance is normalized to 1 are given by

$$J_i' = \frac{J_i}{\sqrt{Y}} \quad i = 0, 1, \ldots, n \quad (23)$$

Since inverter J_0 has no special features, we would have obtained the same result using the input admittance of any other inverter looking from the load towards the admittance Y. Therefore, no matter how many inverters are connected to an admittance, the normalizing factor for node scaling is always $\sqrt{Y}$. If we want to normalize a capacitor, C as in section III-B, then the factor $\sqrt{C}$ appears in the denominator of the expression of any adjacent inverter.

APPENDIX B
ACRONYMS
Due to the extensive use of abbreviations in this work, a table with the acronyms is provided for the reader's convenience. Table 1 provides the meaning for all acronyms in alphabetical order.

REFERENCES
[1] G. L. Matthaei, L. Young, and E. M. T. Jones, *Microwave Filters, Impedance-Matching Networks, and Coupling Structures*. Norwood, MA, USA: Artech House, 1980.
[2] R. J. Cameron, C. M. Kudsia, and R. R. Mansour, *Microwave Filters for Communication Systems: Fundamentals, Design and Applications*, 2nd ed. Hoboken, NJ, USA: Wiley, 2018.
[3] H. Fenech, S. Amos, A. Tomatis, and V. Soumpholphakdy, "High through-put satellite systems: An analytical approach," *IEEE Trans. Aerosp. Electron. Syst.*, vol. 51, no. 1, pp. 192–202, Jan. 2015.
[4] G. Maral and M. Bousquet, *Satellite Communication Systems*, 3rd ed. Chichester, U.K.: Wiley, 1998.
[5] C. Kudsia, R. Cameron, and W.-W. Tang, "Innovations in microwave filters and multiplexing networks for communications satellite systems," *IEEE Trans. Microw. Theory Techn.*, vol. 40, no. 6, pp. 1133–1149, Jun. 1992.
[6] S. Amari and U. Rosenberg, "The doublet: A new building block for modular design of elliptic filters," in *Proc. 32nd Eur. Microw. Conf.*, Oct. 2002, pp. 1–3.
[7] U. Rosenberg and S. Amari, "Novel coupling schemes for microwave resonator filters," *IEEE Trans. Microw. Theory Techn.*, vol. 50, no. 12, pp. 2896–2902, Dec. 2002.
[8] S. Amari and U. Rosenberg, "A universal building block for advanced modular design of microwave filters," *IEEE Microw. Wireless Compon. Lett.*, vol. 13, no. 12, pp. 541–543, Dec. 2003.
[9] S. Moretti, F. Alessandri, and R. Sorrentino, "Field theory design of a nove circular waveguide dual mode filter," in *Proc. 25th Eur. Microw. Conf.*, Oct. 1995, pp. 779–783.
[10] M. Guglielmi, P. Jarry, E. Kerherve, O. Roquebrun, and D. Schmitt, "A new family of all-inductive dual-mode filters," *IEEE Trans. Microw. Theory Techn.*, vol. 49, no. 10, pp. 1764–1769, Oct. 2001.
[11] M. M. Darwish, A. M. El-Tager, H. N. Ahmed, and H. S. El-Hennawy, "Design of in-line dual-mode rectangular waveguide bandpass filters using multiple inductive circular posts," in *Proc. 38th Eur. Microw. Conf.*, Oct. 2008, pp. 500–503.
[12] S. Amari and U. Rosenberg, "New building blocks for modular design of elliptic and self-equalized filters," *IEEE Trans. Microw. Theory Techn.*, vol. 52, no. 2, pp. 721–736, Feb. 2004.
[13] C. Tomassoni, S. Bastioli, and R. Sorrentino, "Generalized TM dual-mode cavity filters," *IEEE Trans. Microw. Theory Techn.*, vol. 59, no. 12, pp. 3338–3346, Dec. 2011.
[14] P. Zhao and K. Wu, "Waveguide filters with central-post resonators," *IEEE Microw. Wireless Compon. Lett.*, vol. 30, no. 7, pp. 657–660, Jul. 2020.
[15] M. Almalkawi, M. Westrick, V. Devabhaktuni, M. Alam, L. Zhu, and J. Deng, "Design of a dual-band dual-mode substrate integrated waveguide filter with symmetric transmission zeros," in *Proc. IEEE Appl. Electro-magn. Conf. (AEMC)*, Dec. 2011, pp. 1–3.
[16] R. Li, X. Tang, and F. Xiao, "Design of substrate integrated waveguide transversal filter with high selectivity," *IEEE Microw. Wireless Compon. Lett.*, vol. 20, no. 6, pp. 328–330, Jun. 2010.
[17] L. Silvestri, C. Tomassoni, A. Ghiotto, M. Bozzi, and L. Perregrini, "Innovative filters in partially air-filled in substrate integrated waveguide technology," in *IEEE MTT-S Int. Microw. Symp. Dig.*, May 2019, pp. 1–3.
[18] C. Tomassoni, G. Venanzoni, M. Dionigi, and R. Sorrentino, "Additive manufacturing of a very compact doublet structure with asymmetric filtering function," in *IEEE MTT-S Int. Microw. Symp. Dig.*, Jul. 2018, pp. 1–3.
[19] C. Tomassoni, G. Venanzoni, M. Dionigi, and R. Sorrentino, "A very compact 3D-printed doublet structure based on a double iris and a pair of slanting rods," in *IEEE MTT-S Int. Microw. Symp. Dig.*, Jun. 2018, pp. 1103–1105.
[20] C. Tomassoni, L. Silvestri, N. Delmonte, M. Bozzi, L. Perregrini, S. Marconi, G. Alaimo, and F. Auricchio, "A new class of doublet based on slotted slant ridge in additive manufacturing technology," in *IEEE MTT-S Int. Microw. Symp. Dig.*, Jul. 2019, pp. 10–12.
[21] R. Mikase, M. Ohira, Z. Ma, and X. Wang, "A novel microstrip symmetric diagonal cross-coupling quadruplet bandpass filter using even/odd-mode stepped impedance resonators," in *IEEE MTT-S Int. Microw. Symp. Dig.*, Jun. 2018, pp. 712–715.
[22] S. Tamiazzo and G. Macchiarella, "An analytical technique for the synthesis of cascaded N-tuplets cross-coupled resonators microwave filters using matrix rotations," *IEEE Trans. Microw. Theory Techn.*, vol. 53, no. 5, pp. 1693–1698, May 2005.
[23] R. J. Cameron, "General prototype network synthesis methods for microwave filters," *ESA J.*, vol. 6, pp. 193–206, Jan. 1982.
[24] S. Cogollos, M. Brumos, V. E. Boria, C. Vicente, J. Gil, B. Gimeno, and M. Guglielmi, "A systematic design procedure of classical dual-mode circular waveguide filters using an equivalent distributed model," *IEEE Trans. Microw. Theory Techn.*, vol. 60, no. 4, pp. 1006–1017, Apr. 2012.
[25] G. Conciauro, M. Guglielmi, and R. Sorrentino, *Advanced Modal Analysis*. Chichester, U.K.: Wiley, 2000.
[26] J. C. Melgarejo, J. Ossorio, S. Cogollos, M. Guglielmi, V. E. Boria, and J. W. Bandler, "On space mapping techniques for microwave filter tuning," *IEEE Trans. Microw. Theory Techn.*, vol. 67, no. 12, pp. 4860–4870, Dec. 2019.
[27] J. Ossorio, J. C. Melgarejo, V. E. Boria, M. Guglielmi, and J. W. Bandler, "On the alignment of low-fidelity and high-fidelity simulation spaces for the design of microwave waveguide filters," *IEEE Trans. Microw. Theory Techn.*, vol. 66, no. 12, pp. 5183–5196, Dec. 2018.

SANTIAGO COGOLLOS (Member, IEEE) was born in Valencia, Spain, in 1972. He received the ''Ingeniero Superior de Telecomunicación'' and ''Doctor Ingeniero de Telecomunicación'' degrees from the Universitat Politècnica de València (UPV), Valencia, Spain, in 1996 and 2002, respectively.

In 2000, he joined the Communications Department, UPV, where he was an Assistant Lecturer, from 2000 to 2001, a Lecturer, from 2001 to 2002, and became an Associate Professor, in 2002. He has collaborated with the European Space Research and Technology Centre of the European Space Agency in the development of modal analysis tools for payload systems in satellites. In 2005, he held a postdoctoral research position working in the area of new synthesis techniques in filter design at the University of Waterloo, Waterloo, ON, Canada. His current research interests include applied electromagnetics, mathematical methods for electromagnetic theory, analytical and numerical methods for the analysis of microwave structures, and design of waveguide components for space applications.

RICHARD J. CAMERON (Life Fellow, IEEE) received the B.Sc. degree in telecommunications and electronic engineering from Loughborough University, U.K., in 1969. In 1969, he joined Marconi Space and Defence Systems, Stanmore, U.K. His activities there included small earth station design, telecommunication satellite system analysis, and computer-aided microwave circuit and component design for spacecraft telecommunication subsystems. In 1975, he joined the European Space Agency's technical establishment (ESTEC, The Netherlands), where he was involved in the research and development of advanced microwave active and passive components and circuits, with applications to communications, earth resources, deep space, TV broadcast, navigation, and meteorological spacecraft. In 1984, he was involved in the establishment of a European branch of the Com Dev Company of Canada, U.K. He was involved in the development of the technical basis of the company whilst continuing with Research and Development into software and methods for the design of high-performance components and subsystems for both advanced space-borne and terrestrial application. He is a fellow of the U.K. Institution of Engineering and Technology (formerly the IEE).

MARCO GUGLIELMI (Life Fellow, IEEE) was born in Rome, Italy, in December 1954. He received the ''Laurea in Ingegneria Elettronica'' degree from the University of Rome ''La Sapienza,'' Rome, in 1979, the M.S. degree in electrical engineering from the University of Bridgeport, Bridgeport, CT, USA, in 1982, the Ph.D. degree in electrophysics from Polytechnic University, Brooklyn, NY, USA, in 1986.

He also attended the ''Scuola di Specializzazione in Elettromagnetismo Applicato,'' University of Rome ''La Sapienza,'' in 1980. From 1984 to 1986, he was an Academic Associate at Polytechnic University, and from 1986 to 1988, he was an Assistant Professor with Polytechnic University. From 1988 to 1989, he was an Assistant Professor at the New Jersey Institute of Technology, Newark, NJ, USA. In 1989, he joined the RF System Division, European Space Agency, European Space Research and Technology Centre (ESTEC), Noordwijk, The Netherlands, as a Senior Microwave Engineer, where he was in charge of the development of microwave filters and electromagnetic simulation tools. In 2001, he was appointed as the Head of the Technology Strategy Section, ESTEC, where he contributed to the development of management processes and tools for the formulation of a European strategy for Space Technology Research and Development. In 1981, he was awarded a Fulbright Scholarship in Rome, and an Halsey International Scholarship Program (HISP) from the University of Bridgeport. In 2014, he retired from the European Space Agency and is currently an Invited Senior Researcher at the Polytechnic University of Valencia, Valencia, Spain. He has been elevated to the grade of a fellow of the IEEE ''For Contributions to Multimode Equivalent Networks and Microwave Filter Design,'' in January 2013.

JUAN CARLOS MELGAREJO was born in Alicante, Spain, in 1993. He received the bachelor's, dual master's, and Ph.D. degrees in telecommunications engineering from the Universitat Politècnica de València, Spain, in 2015, 2019, and 2021, respectively. He is currently working as a Machine Learning Engineer at Cambrian Intelligence. His main research interests include investigating microwave passive devices and new manufacturing techniques for satellite components.

VICENTE E. BORIA (Fellow, IEEE) was born in Valencia, Spain, in May 1970. He received the ''Ingeniero de Telecomunicación'' (Hons.) and the ''Doctor Ingeniero de Telecomunicación'' degrees from the Universidad Politècnica de València, Valencia, Spain, in 1993 and 1997, respectively.

In 1993, he joined the ''Departamento de Comunicaciones,'' Universidad Politècnica de València, where he has been a Full Professor, since 2003. In 1995 and 1996, he was holding a Spanish Trainee position with the European Space Research and Technology Centre, European Space Agency (ESTEC-ESA), Noordwijk, The Netherlands, where he was involved in the area of EM analysis and design of passive waveguide devices. He has authored or coauthored ten chapters in technical textbooks, 180 articles in refereed international technical journals, and over 200 papers in international conference proceedings. His current research interests include the analysis and automated design of passive components, left-handed and periodic structures, as well as on the simulation and measurement of power effects in passive waveguide systems.

Dr. Boria has been a member of the IEEE Microwave Theory and Techniques Society (IEEE MTT-S) and the IEEE Antennas and Propagation Society (IEEE AP-S), since 1992. He is also a member of the Technical Committees of the IEEE-MTT International Microwave Symposium and of the European Microwave Conference. He is also a member of the European Microwave Association (EuMA). He has been the Chair of the 48th European Microwave Conference held in Madrid, Spain. He acts as a regular reviewer of the most relevant IEEE and IET technical journals on his areas of interest. He has been an Associate Editor of the IEEE Microwave and Wireless Components Letters (2013–2018) and *IET Electronics Letters* (2015–2018). He serves as a Subject Editor (Microwaves) of *IET Electronics Letters*, and as an Editorial Board Member of the *International Journal of RF and Microwave Computer-Aided Engineering*.

• • •